Volume 1 | Number 1 | Jan 2013 | Pages 1–100

Journal of
Materials Chemistry C

Materials for optical and electronic devices
www.rsc.org/materialsC

ROYAL SOCIETY
OF CHEMISTRY

ROYAL SOCIETY
OF CHEMISTRY

www.rsc.org/materialsC

Color Tuning in Inverted Blue Light-Emitting Diodes Based on Polyfluorene Derivative by Adjusting the Thickness of Light-Emitting Layer

Jin Xu, Lei Yu, Liwen Hu, Ruifeng He,* Wei Yang,* Junbiao Peng and Yong Cao

Institute of Polymer Optoelectronic Materials and Devices, State Key Lab of Luminescent Materials and Devices, South China University of Technology, Guangzhou 510640, China

Corresponding Author: Wei Yang

E-mail: pswyang@scut.edu.cn; msrfhe@scut.edu.cn

ABSTRACT:

Inverted blue polymer light-emitting diodes (IPLEDs) were fabricated by using polyethylenimine ethoxylated (PEIE) as the interlayer and polyfluorene derivative (PF-FSO10) as the emissive layer, with the device structure of ITO/ZnO/PEIE/PF-FSO10/MoO$_3$/Al. With insetting the PEIE interlayer, the maximum luminous efficiency (LE$_{max}$) of the IPLEDs increase about three order of magnitude, compared with that without. The enhancement of device performances could be attributed to the effective electron-injecting/hole-blocking ability of PEIE, and less exciton quenching at the interface of ITO/ZnO/PEIE. As tuning the thickness of PF-FSO10, the color coordinate of the devices can change from sky blue (0.18,0.26) to deep blue (0.16,0.07), and the LE$_{max}$ of the devices can also be improved from 1.77 to 5.7 cd A^{-1}，which should be contributed to the micro-cavity effects and the expansible recombination zone, respectively. This results provide an excellent method to improve the efficiency and color purity of the inverted blue-light emitting diodes.

Keywords：polyfluorene, blue-emission, PEIE, micro-cavity effect, IPLED

1. Introduction

Polymer light-emitting diodes (PLEDs) have attracted great attention due to their broad application potential in full-color flat-panel electroluminescence (EL) displays, back-lighting sources for liquid-crystal displays and next-generation solid-state lighting sources.[1-4] Among the primary colors of red, green and blue (RGB), the blue light emission is recognized as a shortcoming for PLEDs, mainly due to its device stability, efficiency and poor color purity.[5, 6] As specified by the National Television System Committee (NTSC) standard, the CIE coordinates of the blue EL should be (0.14, 0.08) for meeting the demand of full-color display.[7] Although various blue emitting luminescent materials have been designed and synthesized, however, neither the device stability and efficiency nor the color purity could achieve desirable results.[8, 9] In order to solve those problems, advanced method for device structure optimization can be a good choice, compared with the complex material design and chemical synthesis.

In the matter of device stability, in conventional PLEDs (CPLEDs), using PEDOT:PSS and low work function metals will badly harm the stability of device.[10-13] This problem can be subtly avoided in inverted polymer emitting diodes (IPLEDs). IPLEDs possess innate advantage on device stability, due to the emissive layer embed between p-type and n-type metal oxide, which can separate oxygen and moisture efficiently.[14] The p-type metal oxide, e.g. MoO_3, WO_3, V_2O_5 and NiO, are used as a hole injection/transport layer, which have excellent chemical stability, high charge carrier mobility and high optical transmittance.[15-21] The n-type metal oxide, such as ZnO, TiO_2, MgO, HfO_2 and ZrO_2, are used as electron injection/transport layer in IPLEDs. [22-27]

To improve the device efficiency, one of the popular methods is using suitable interface materials, such as Cs_2CO_3, $Ba(OH)_2$, conjugated polyelectrolyte FPQ-Br and amine-based polar solvent, to modify n-type metal oxide in IPLEDs.[28-32] Thereinto, non-conjugated polymer PEIE can be an excellent candidate as the interface material for IPLEDs, with its advantages of excellent stability in the atmosphere and being able to reduce the work function of conductors including metals, metal oxides, and grapheme.[33] Additionally, PEIE have been used as ZnO interlayer and obtained highly efficient light-emitting diodes due to the improvement of electron injection. [34-36]

For tuning the color purity, the micro-cavity effects may be a magic tool. The micro-cavity structure, named Fabry-Pérot cavity, commonly consists of a reflective electrode, a semi-transparent electrode and emissive layer.[37] Cheung et al. discovered that changing the

thickness of light-emitting layer could acquire the emission spectra with different main peak.[38] Such strange phenomenon should be caused by optical interference, which was generated from the light emitting directly out of device through glass substrate and reflecting off of the metal cathode.[39] Bulovic et al. changed the thickness of light-emitting material Alq3 from 20 nm to 50 nm in conventional organic light-emitting devices, resulting in the emission peak changed from 530 nm to 545 nm, which was concluded to be weak micro-cavity effects.[40] Wherein, Alq3 is an *n*-type material, as a result, the recombination zone should be far away from the metal electrode Ag (cathode).

Actually, all of the PLEDs possess micro-cavity, however, relative reports were quite a few, because most of luminescent materials are *p*-type materials, and the recombination zone is near to the metal electrode, resulting in the effects on the micro-cavity can be normally ignored without additional semi-transparent mirror. Developing the no semi-transparent electrode micro-cavity is still a great challenge. Specially, in IPLEDs, the hole injected from the metal electrode, therefore, the recombination zone of the device with *p*-type emitting materials is far away from the metal electrode, which is beneficial to generate the micro-cavity.

Based on the above consideration, we fabricated a series of IPLEDs by using PEIE as the interlayer and blue light emitting polyfluorene (PF-FSO10) as the emitting layer, with the device structure of ITO/ZnO/PEIE/PF-FSO10/MoO$_3$/Al. Wherein, PF-FSO10 with excellent light-emitting electroluminescence properties matched HOMO level (-5.9 eV) with MoO$_3$.[29, 41] The device performance and color purity were fully analyzed by adjusting the thickness of the PEIE and PF-FSO10.

2. Experimental Section

Materials: The blue light-emitting poly(9,9-dioctyl-2,7-fluorene-*co*-3,7-dibenzothiopene -*S,S*-dioxide) (PF-FSO5 and PF-FSO10), poly(9,9-bis(4-(2-ethyl-hexyloxy)phenyl)-2,7-fluorene -*co*-3,7-dibenzothiopene-*S,S*-dioxide-*co*-4,7-benzothiadiazole) (PPF-FSO10-BT2), poly(9,9-bis(4-(2-ethyl-hexyloxy)phenyl)-2,7-fluorene-*co*-3,7-dibenzothiopene-*S,S*-dioxide-*co*-5,5 '-(4,7-di(4-hexylthien-2-yl)-benzothiadiazole)) (PPF-FSO25-DHTBT10) were synthesized according to reported procedures.[41, 42] The Zinc acetate, dehydrate, Molybdenum(VI) oxide and PEIE (M$_w$ = 70000 g mol^{-1}) were purchased from Aldrich.

PLED fabrication and measurements: The fabrication of the inverted polymer light-emitting diodes (IPLEDs) followed a well-established process. The ITO glass substrates with a sheet resistance of 15–20 ohm/square were cleaned in an ultrasonic bath successively in acetone, detergent, deionized water, and isopropanol. After a 40 nm-thick ZnO layer was prepared on the precleaned ITO by using sol-gel method described previously,[43] PEIE (dissolved in 2-methoxythanol with different concentration) was spin-coated with different speed, then the PEIE layer were annealed at 120 °C for 10 min on the atmosphere. PF-FSO10 emissive layer was spin-coated from a p-xylene solution to form a uniform film with a wide range of thickness from 100 to 700nm on top of the PEIE layer, then annealed at 100 °C on a hotplate for 20 min. Finally, 10 nm of MoO_3 followed by 120 nm of aluminum were thermally evaporated through a shadow mask at a base pressure of 2.0×10^{-6} mbar to form the cathode. Overlap between the cathode and anode defined the 0.16 cm^{-2} pixel area.

The hole-only and electron-only devices structure were ITO/PEDOT:PSS/PF-FSO10/MoO_3/Al and ITO/ZnO/PEIE(with or without)/PF-FSO10/CsF/Al, respectively. To fabricate the hole-only device, after oxygen plasma treatment, a 40 nm-thick PEDOT:PSS layer was spin-coated directly on the ITO substrate and annealed at 120 °C on a hot plate for 20 min. PF-FSO10 emission layer was spin-coated in p-xylene to form a uniform film on top of the PEDOT:PSS layer, then annealed at 100 °C on a hotplate for 20 min. Finally, 10 nm of MoO_3 followed by 120 nm of aluminum were thermally evaporated through a shadow mask at a base pressure of 2.0×10^{-6} mbar to form the cathode. For the electron-only device, ITO glass substrate was deposited with a layer of ZnO (40 nm) to replace the PEDOT:PSS film, then a 100 nm thick polymer layer was spin-cast from p-xylene solution on top of the ZnO layer and annealed at 100 °C for 20 min. Finally, 1.5 nm of CsF followed by 120 nm of aluminum were thermally evaporated through a shadow mask at a base pressure of 2.0×10^{-6} mbar to form the electrode.

The thicknesses of the polymer, PEDOT:PSS and ZnO were determined by a Tencor Alpha-step 500 Surface Profilometer. The thicknesses of the PEIE were measured on Si wafer substrate by spectroscopic ellipsometer (J. A. Woollam Co.). And the thicknesses of MoO_3 and Al were monitored with a STM-100/ MF Sycon quartz crystal. The current density-luminance-voltage (J–L–V) characteristics were measured in the nitrogen dry-box using a Keithley 236 source-measurement unit and a calibrated silicon photodiode. The

electroluminescence (EL) spectra and CIE color coordinates were recorded using PR-705 Spectrascan spectrophotometer (Photo Research). EL spectra with different viewing angles were measured with PR-705 by changing the angle between IPLED and PR-705. Atomic force microscopy (AFM) images were recorded in tapping mode on NanoScopeIII system**.** The PL quantum yields were measured using an Integrating Sphere IS080 (LabSphere) to collect the emitted light in all directions under the excitation of 325 nm HeCd laser (MellesGriot). Transient PL was measured with an Edinburgh FL920 fluorescence spectrophotometer.

3. Results and Discussion

3.1 Enhancement of Efficiency by Adopting PEIE Interlayer

Chemical structures of PF-FSO10 and PEIE were showed in **Fig. 1**. The PEIE's thickness was firstly optimized, in considering which had significance effect on device performance. And the device with a configuration of ITO/ZnO/PEIE(x nm)/PF-FSO10(100 nm)/MoO$_3$/Al were fabricated, wherein x was 0, 6.7, 9.1, 11.7 and 13.2, corresponding to the device A, B, C, D and E, respectively, by controlling the processing conditions.

The detailed characteristics are summarized in **Table 1**. For device A, the maximum luminous efficiency (LE$_{max}$) and the maximum luminance (L$_{max}$) were 3.3×10^{-3} cd A^{-1} and 20 cd m^{-2}, respectively, and the turn-on voltage (V$_{on}$) was as high as 6.5 V. By adding 6.70 nm PEIE interlayer (device B), all the device performance parameters were simultaneously improved, with an LE$_{max}$ of 1.33 cd A^{-1}, L$_{max}$ of 4524 cd m^{-2} and V$_{on}$ of 3.25 V. For the optimized thickness (device C), the device performance got further improvement with an LE$_{max}$ of 3.16 cd A^{-1}, which can equal the standard of CPLED.[41] The internal reasons for the dramatic improvements were analyzed by following.

Firstly, atomic force microscopy (AFM) test was used to detect the microcosmic structure of the interface. And the height images of the films are shown in **Fig.2**. The surface roughness of root-mean-square (RMS) recorded for ZnO (ITO/ZnO) was 1.61 nm, and reducing to 0.97 nm after inserting the PEIE interlayer. Secondly, the single charge carrier devices were fabricated to investigate the effect of PEIE on electron-injecting/hole-blocking with the configuration of ITO/PEDOT:PSS/PF-FSO10/MoO$_3$/Al(hole-only device) and ITO/ZnO/PEIE(with or without)/PF-FSO10/CsF/Al (electron-only device), respectively. **Fig. 3a** shows the current density

versus voltage (J-V) characteristics of hole-only and electron-only devices, respectively. It can be found that the hole current is three orders of magnitudes larger than electron current, as a result, promoting the electron injection can be a key point for balancing the carrier transport and improving the performance of the hole-dominant IPLEDs. By inserting the PEIE layer, the electron current was prominently enhanced, leading to a dramatic improvement in the device performances. **Fig. 3b** shows the J-V characteristics of the hole-only device and the IPLED device with or without PEIE. The current density without PEIE (A) was similar to that of the hole-only devices. At the voltage of 1 V, there existed a threshold for current onset and above this voltage, the current increased rapidly, which indicated that ZnO possessed insufficient hole-blocking ability. For the device with PEIE(C), the threshold voltage increased to 2.5 V, which implied that the hole-blocking ability had remarkable improvement by inserting PEIE. Similar behaviors had also been demonstrated when ZnO film was modified by Cs_2CO_3 or $Ba(OH)_2$.[30, 44] Finally, the photoluminescence (PL) quantum efficiency (Φ_{PL}) of the polymer in different interfaces were measured by an integrating sphere (in **Table 2**) to estimate whether PEIE layer can block exciton quenching.[45] Considering the recombination zone next to the PEIE interface, the exciton generated by photo excitation should get to the PEIE interface, which can simulate the situation of device operate as accurate as possible.

Hence，the thickness of PF-FSO10 was selected as 10 nm, which was the estimated exciton diffusion length in PF-FSO10 film.[34, 46] The Φ_{PL} of PF-FSO10 based on the interface of ITO/ZnO/PF-FSO10 is 24%, indicating serious exciton quenching compared with 47% on the quartz. Comparably, the Φ_{PL} on the interface of ITO/ZnO/PEIE(9.1 nm) /PF-FSO10 is about 34 %, implying that inserting PEIE layer on the ZnO would decrease exciton quenching to the utmost extent. Therefore，the improvement of the device performances can be attributed to the superior electron-injecting/hole-blocking ability of PEIE and reduced exciton quenching.

The luminous efficiency roll-off rates are the important judgment for the devices. From the luminous efficiency-current density (LE-J) characteristics of the device A, B, C, D and E (**Fig. 4**), it can be found that the device performances were close linked with the PEIE's thickness. And the decay rate of efficiency will increase rapidly with the increasing thickness of PEIE (device D and E). It is well known that the efficiency roll-off rates are mainly caused by the variation of exciton lifetime,[47] exciton recombination zone[48] and exciton quenching triggered by charge accumulation

at the interface .[49-51]

On the one hand, exciton lifetime with different thickness of PEIE was determined by time-correlated single-photon counting. The exciton lifetime from ITO/ZnO/PEIE(9.1nm)/PF-FSO10 and ITO/ZnO/PEIE(13.2 nm)/PF-FSO10 are 2.30 ns and 2.32 ns, respectively (**Fig. 5a**), indicating that exciton lifetime would not be obviously changed for different thickness of PEIE. In other words, exciton lifetime effect could be neglected from the causes of the efficiency roll-off rates in these devices. On the other hand, the electroluminescence (EL) spectra (**Fig. 5b**), detected by spectrophotometer, almost remain unchanged with varying the thickness of PEIE layer, implying that the exciton recombination zone is not altered. Thereby, exciton quenching, triggered by charge accumulation at the PEIE interface, could be the most likely cause for the different efficiency roll-off rates in these IPLEDs.

The J-V characteristics of IPLEDs with different thickness of PEIE are shown in **Fig. 6**. With increasing the thickness of PEIE, the current densities are decreased, indicating that the hole-blocking ability of PEIE is enhanced and more hole carriers are accumulated at the interface, resulting in intensifying the efficiency roll-off. When the PEIE thickness of 6.7 nm (device B), the device showed superior performances compared with that without PEIE (device A), and the efficiency roll-off is slight with the increase of current density. Moreover, the LE get further improvement with PEIE thickness of 9.1 nm (device C), which can be contributed to the enhancement of hole-blocking ability. However, the device performances fell badly with a thicker PEIE layer (D:11.7 nm or E:13.2 nm), due to the further enhancement of hole-blocking capability and the reduction of electron-injecting capability, determined by the weak charge-transport ability of unconjugated backbone of PEIE.[34] Resultingly, more hole carrier would be accumulated at the interface, then increasing the efficiency roll-off rates. Thus, appropriate thickness of PEIE has played an important role in balancing hole-blocking and electron-injecting for high-performance IPLEDs.

3.2 Improvement of Color Purity by Adjusting the Emissive Layer's Thickness

The EL spectra of F8BT can be tuned from green to orange emission (550 nm to 610 nm) by adjusting the thickness of hole-transporting layer in the IPLEDs derived from recently reports.[52] The variation of EL spectra was attributed to micro-cavity effects. Moreover, the LE of about 28

cd A^{-1} can be made with 1.2 um-thick F8BT due to the expansible recombination zone in the IPLEDs.[28, 30]

Referring this amazing phenomenon, it deserved to try to optimize the thickness of PF-FSO10, no matter for improving the color purity or the device efficiency. And the IPLEDs were prepared, with the thickness of emissive layer ranging from 100 nm to 700 nm. Detailed device parameters and EL spectra with the different thickness are summarized in **Fig.7 (a)** and **Table 2**. It can be found that a deep blue emission with CIE (0.16,0.07) and an EQE of 3.23% was obtained in the emissive layer thickness of 134 nm. And as the thickness increased to 700 nm, the device reached the highest EQE of 5.83% (LE$_{max}$ of 5.70 cd A^{-1}) with a CIE coordinate of (0.16,0.16). Moreover, the EL spectra shifted from peaked at 474 nm to 444 nm, along with the emitting color adjusted from sky-blue to deep-blue emission. As shown in the **Fig. 7(b)**, it is clearly that the CIE$_{X+Y}$ (the sum of color coordinate X and Y) oscillate between 0.2 and 0.4. And it is necessary to find out the real reason of the amazing phenomenon. Optical interference[39, 53-55] combining with micro-cavity effects could be the most likely cause.[40, 52] The curves of J-V-L and LE-J characteristics are shown in **Fig.S2 (a, c)**. EL spectra with the different emitting layer's thickness vs. the current densities are shown in **Fig.8**. We can see that both EL spectra and CIE coordinates exhibit no obvious change even in the large driving current densities of 12-300 mA cm^{-2}, which shows an excellent EL spectral stability.

The EL spectra for different viewing angles were measured to confirm whether micro-cavity effects existing in the IPLED. And the results are shown in **Fig. 9**. The EL spectra appear narrowing with increasing the viewing angles, indicating that there exist strong micro-cavity effects in the IPLEDs.[56, 57] According to the analysis of single charge carrier devices, it could be concluded that the recombination zone occurred in the cathode interface, due to the absolutely dominant hole carrier in the IPLEDs. It also means that the recombination area should be far away from the metal electrode in the IPLEDs. And the recombination zone would gradually away from metal electrode with increasing the thickness of emissive layer in IPLEDs. Therefore, the emissive spectra would change with the varying recombination area.[58, 59]

More specifically, the optical interference can change the emissive spectra easily. And the most important interference effect occurs between the light emitted directly out of the device

through ITO substrate and the light reflected back by the metal electrode.[39] In IPLEDs, the recombination zone is close to the PEIE/PF-FSO10 interface, bringing that a half of photon in probability statistics maybe go across the light-emitting layer to metal anode aluminum, then reflect back and go across the light-emitting layer again. The optical path difference between photon reflected back from aluminum and photon emitted directly out from glass substrate has significance effect on optical interference. Detailed explanation about optical interference is shown in supporting information. We also studied whether analogous phenomenon appears in the CPLEDs. And the J-V-L and J-LE characteristics of different emissive layer's thickness are shown in **Fig.S2 (b** and **d).** Unlike in the IPLEDs, the EL spectra (in **Fig.S3 (a)**) almost kept the similar with the variation of thickness in the CPLEDs.

The main reason could be the recombination zone closed to the metal cathode in the CPLEDs. The small optical path for the light reflected back by the metal electrode was not satisfied the condition of optical interference, resulted in little optical interference effect with the variation of emissive layer's thickness. Therefore, the location of recombination zone plays a decisive role the micro-cavity effects with the bottom-emitting OLED without semi-transparent electrode. If the recombination zone is far away from the metal electrode, the micro-cavity effects will strength greatly in the bottom-emitting OLED. On the contrary, the micro-cavity effects can be neglected.

Other RGB light emitting polyfluorene derivatives PF-FSO5, PPF-FSO10-BT2 and PPF-FSO25-DHTBT10 were also used for analyzing the EL spectra in the inverted structure device. And the relative EL spectra are shown in **Fig.S3 (b, c** and **d)**. The variation of EL spectra was similar to the PF-FSO10 based IPLEDs. In **Fig.S3**, the spectra tendency of RGB light-emitting polymers has a oscillatory variation with the increase of emitting layer's thickness, which are from narrowing to broadening(b), from broadening to narrowing (c), and from broadening to narrowing (d), respectively. It is because, in the IPLEDs, that the variation in emission may be not only attributed to micro-cavity effect, but also to other factors, such as a number of interfaces are present in the device, and the variation in refractive index (*n*). [52, 60]

4. Conclusion

By adding a solution-processed PEIE interlayer，the device efficiencies were significantly improved, owing to the electron-injecting/hole-blocking ability of PEIE and reduction of the

exciton quenching at the PEIE interface. The thickness of the PEIE would affect the roll-off of LE, due to the exciton quenching triggered by charge accumulation at the PEIE interface. And with the contribution of the micro-cavity effects and the expansible recombination zone, the light emission could be tuned from sky blue (0.18,0.26) to deep blue (0.16,0.07) by changing the thickness of the emissive layer.

Acknowledgments

References

1   J. H. Burroughes, D. D. C. Bradley, A. R. Brown, R. N. Marks, K. Mackay, R. H. Friend, P. L. Burns and A. B. Holmes, *Nature.*, 1999, **347**, 539-541.

2   R. H. Friend, R. W. Gymer, A. B. Holmes, J. H. Burroughes, R. N. Marks, C. Taliani, D. D. C. Bradley, D. A. D. Santos, J. L. Bredas, M. Logdlund and W. R. Salaneck, *Nature.*, 1999, **397**, 121-128.

3   B. W. D. Andrade and S. T. Forrest, *Adv. Mater.*, 2004, **16**, 1585-1595.

4   H. B. Wu, L. Ying, W. Yang and Y. Cao, *Chem .Soc .Rev.*, 2009, **38**, 3391-3400.

5   B. Chen, J. Ding, L. Wang, X. Jing and F. Wang, *Chem. Commun.*, 2012, **48**, 8970-8972.

6   X. Yang, X. Xu and G. Zhou, *J. Mater. Chem. C.*, 2014, **3**, 913-944.

7   L. Wang, Y. Jiang, J. Luo, Y. Zhou, J. H. Zhou, J. Wang, J. B. Peng and Y. Cao, *Adv. Mater.*, 2009, **21**, 4854-4858.

8   K. Zhang, C. M. Zhong, S. J. Liu, A. H. Liang, S. Dong and F. Huang, *J. Mater. Chem. C.*, 2014, **2**, 3270-3277.

9   M. Yu, S. Wang, S. Shao, J. Ding, L. Wang, X. Jing and F. Wang, *J. Mater. Chem. C.*, 2015, **3**, 861-869.

10   M. P. de Jong, L. J. van Ijzendoorn and M. J. A. de Voigt, *Appl. Phys. Lett.*, 2000, **77**, 2255-2257.

11   K. W. Wong, H. L. Yip, Y. Luo, K. Y. Wong, W. M. Lau, K. H. Low, H. F. Chow, Z. Q. Gao, W. L. Yeung and C. C. Chang, *Appl. Phys. Lett.*, 2002, **80**, 2788-2790.

12   P. E. Burrows, V. Bulovic, S. R. Forrest, L. S. Sapochak, D. M. McCarty and M. E. Thompson, *Appl. Phys. Lett.*, 1994, **65**, 2922-2924.

13   Y.-F. Liew, H. Aziz, N.-X. Hu, H. S.-O. Chan, G. Xu and Z. Popovic, *Appl. Phys. Lett.*, 2000, **77**, 2650-2652.

14   M. Sessolo and H. J. Bolink, *Adv. Mater.*, 2011, **23**, 1829-1845.

15   I. M. Chan and F. C. Hong, *Thin Solid Films.*, 2004, **450**, 304-311.

16   J. Li, M. Yahiro, K. Ishida, H. Yamada and K. Matsushige, *Synth. Met.*, 2005, **151**, 141-146.

17 H. C. Im, D. C. Choo, T. W. Kim, J. H. Kim, J. H. Seo and Y. K. Kim, *Thin Solid Films.*, 2007, **515**, 5099-5102.

18 J. Wu, J. Hou, Y. Cheng, Z. Xie and L. Wang, *Semicond. Sci. Technol.*, 2007, **22**, 824-826.

19 H. M. Zhang and W. C. Choy, *IEEE. T .Electron. Dev.*, 2008, **55**, 2517-2520.

20 J. Meyer, T. Winkler, S. Hamwi, S. Schmale, H.-H. Johannes, T. Weimann, P. Hinze, W. Kowalsky and T. Riedl, *Adv. Mater.*, 2008, **20**, 3839-3843.

21 K. Zilberberg, S. Trost, H. Schmidt and T. Riedl, *Adv. Energy. Mater.*, 2011, **1**, 377-381.

22 H. J. Bolink, H. Brine, E. Coronado and M. Sessolo, *Adv. Mater.*, 2010, **22**, 2198-2201.

23 B. R. Lee, H. Choi, J. SunPark, H. J. Lee, S. O. Kim, J. Y. Kim and M. H. Song, *J. Mater. Chem.*, 2011, **21**, 2051-2053.

24 H. J. Bolink, E. Coronado, D. Repetto, M. Sessolo, E. M. Barea, J. Bisquert, G. Garcia-Belmonte, J. Prochazka and L. Kavan, *Adv. Funct. Mater.*, 2008, **18**, 145-150.

25 H. W. Choi, S. Y. Kim, W.-K. Kim and J.-L. Lee, *Appl. Phys. Lett.*, 2005, **87**, 082102.

26 H. J. Bolink, H. Brine, E. Coronado and M. Sessolo, *J. Mater. Chem.*, 2010, **20**, 4047-4049.

27 N. Tokmoldin, N. Griffiths, D. D. C. Bradley and S. A. Haque, *Adv. Mater.*, 2009, **21**, 3475-3478.

28 T. -W. Lee, J. Hwang and S. -Y. Min, *ChemSusChem.*, 2010, **3**, 1021-1023.

29 D. Kabra, L. P. Lu, M. H. Song, H. J. Snaith and R. H. Friend, *Adv. Mater.*, 2010, **22**, 3194-3198.

30 L. P. Lu, D. Kabra and R. H. Friend, *Adv. Funct. Mater.*, 2012, **22**, 4165-4171.

31 H. Choi, J. S. Park, E. Jeong, G. H. Kim, B. R. Lee, S. O. Kim, M. H. Song, H. Y. Woo and J. Y. Kim, *Adv. Mater.*, 2011, **23**, 2759-2763.

32 B. R. Lee, E. D. Jung, J. S. Park, Y. S. Nam, S. H. Min, B. S. Kim, K. M. Lee, J. R. Jeong, R. H. Friend, J. S. Kim, S. O. Kim and M. H. Song, *Nat. Commun.*, 2014, **5**, 4840-4847.

33 Y. Zhou, C. Fuentes-Hernandez, J. Shim, J. Meyer, A. J. Giordano, H. Li, P. Winget, T. Papadopoulos, H. Cheun, J. Kim, M. Fenoll, A. Dindar, W. Haske, E. Najafabadi, T. M. Khan, H. Sojoudi, S. Barlow, S. Graham, J. L. Bredas, S. R. Marder, A. Kahn and B. Kippelen, *Science.*, 2012, **336**, 327-332.

34 Y.-H. Kim, T.-H. Han, H. Cho, S.-Y. Min, C.-L. Lee and T.-W. Lee, *Adv. Funct. Mater.*, 2014, **24**, 3808-3814.

35 S. Hofle, A. Schienle, M. Bruns, U. Lemmer and A. Colsmann, *Adv. Mater.*, 2014, **26**, 2750-2754.

36 T. Xiong, F. Wang, X. Qiao and D. G. Ma, *Appl. Phys. Lett.*, 2008, **93**, 123310.

37 S. Chen, L. Deng, J. Xie, L. Peng, L. Xie, Q. Fan and W. Huang, *Adv. Mater.*, 2010, **22**, 5227-5239.

38 C. H. Cheung, A. B. Djurisic, C. Y. Kwong, H. L. Tam, K. W. Cheah, Z. T. Liu, W. K. Chan, P. C. Chui, J. Chan and A. D. Rakic, *Appl. Phys. Lett.*, 2004, **85**, 2944-2946.

39 J. D. Shore, *Appl. Phys. Lett.*, 2005, **86**, 186101.

40 V. Bulovic, V. B. Khalfin, G. Gu, P. E. Burrows, D. Z. Garbuzov and S. R. Forrest, *Phys. Rev. B.*, 1998, **58**, 3730-3740.

41 Y. Li, H.B. Wu, J. Zou, L. Ying, W. Yang and Y. Cao, *Org. Electron.*, 2009, **10**, 901-909.

42 L. Yu, J. Liu, S. J. Hu, R. F. He, W. Yang, H. B. Wu, J. B. Peng, R. Xia and D. D. C. Bradley, *Adv. Funct. Mater.*, 2013, **23**, 4366-4376.

43 T. B. Yang, W. Z. Cai, D. Qin, E. G. Wang, L.F. Lan, X. Gong, J. B. Peng and Y. Cao, *J. Phys. Chem. C.*, 2010, **114**, 6849-6853.

44 H. J. Bolink, E. Coronado, J. Orozco and M. Sessolo, *Adv. Mater.*, 2009, **21**, 79-82.

45 T. C. Monson, M. T. Lloyd, D. C. Olson, Y.-J. Lee and J. W. P. Hsu, *Adv. Mater.*, 2008, **20**, 4755-4759.

46 A. Kohnen, M. Irion, M. C. Gather, N. Rehmann, P. Zacharias and K. Meerholz, *J. Mater. Chem.*, 2010, **20**, 3301-3306.

47 X. Li, D. Zhang, H. Chi, G. Xiao, Y. Dong, S. Wu, Z. Su, Z. Zhang, P. Lei, Z. Hu and W. Li, *Appl. Phys. Lett.*,

2010, **97**, 263303.

48   G. He, M. Pfeiffer, K. Leo, M. Hofmann, J. Birnstock, R. Pudzich and J. Salbeck, *Appl. Phys. Lett.*, 2004, **85**, 3911-3913.

49   S. H. Kim, J. Jang and J. Y. Lee, *Appl. Phys. Lett.*, 2007, **91**, 083511.

50   H. Wang, K. P. Klubek and C. W. Tang, *Appl. Phys. Lett.*, 2008, **93**, 093306.

51   Z. B. Wang, M. G. Helander, Z. W. Liu, M. T. Greiner, J. Qiu and Z. H. Lu, *Appl. Phys. Lett.*, 2010, **96**, 043303.

52   J. C. D. Faria, A. J. Campbell and M. A. McLachlan, *J. Mater. Chem. C.*, 2015, **3**, 4945-4953.

53   Y. Cao, L. D. Parker, G. Yu, C. Zhang and A. J. Heeger, *Nature.*, 1999, **397**, 414-417.

54   C. H. Cheung, A. B. Djurišić, C. Y. Kwong, H. L. Tam, K. W. Cheah, Z. T. Liu, W. K. Chan, P. C. Chui, J. Chan and A. D. Rakić, *Appl. Phys. Lett.*, 2004, **85**, 2944-2946.

55   C. H. Cheung, A. B. Djurišić, C. Y. Kwong, H. L. Tam, K. W. Cheah, Z. T. Liu, W. K. Chan, P. C. Chui, J. Chan and A. D. Rakić, *Appl. Phys. Lett.*, 2005, **86**, 186102.

56   C.-C. Chang, J.-F. Chen, S.-W. Hwang and C. H. Chen, *Appl. Phys. Lett.*, 2005, **87**, 253501.

57   H. Zhang, Y. Dai, D. Ma and H. Zhang, *Appl. Phys. Lett.*, 2007, **91**, 123504.

58   J. Huang, W.-J. Hou, J.-H. Li, G. Li and Y. Yang, *Appl. Phys. Lett.*, 2006, **89**, 133509.

59   M. C. Gather, R. Alle, H. Becker and K. Meerholz, *Adv. Mater.*, 2007, **19**, 4460-4465.

60   M. C. Gather, M Flämmich, N Danz,D Michaelis, K Meerholz1, *Appl. Phys. Lett.*, 2009, 94, 263301.

Figure captions

Fig.1. Chemical structures of PF-FSO10 and PEIE.

Fig.2. AFM height images (5 ×5 μm) in film: ITO/ZnO (a) and ITO/ZnO/PEIE (b).

Fig.3. Current density vs. voltage (J-V) characteristics of the hole-only device: ITO/PEDOT:PSS/PF-FSO10/MoO$_3$/Al and the electron-only devices: ITO/ZnO/(PEIE)/PF-FSO10/CsF/Al(a); J-V characteristics of the hole-only devices and the devices: with/without PEIE interlayer (b).

Fig.4. Luminous efficiency vs. current density (LE-J) characteristics of the devices with the different thickness of PEIE.

Fig.5. Transient PL decay curves in film (a) and EL spectra of the devices with the different thickness of PEIE (b).

Fig.6. J-V characteristics of the devices with the different thickness of PEIE.

Fig.7. EL spectra (a) and CIE$_{X+Y}$ (b) with the different thickness of emissive layer.

Fig.8. EL spectra of PF-FSO10 vs. the applied current densities with the different thickness of emissive layer.

Fig.9. EL spectra of PF-FSO10 based on the different viewing angles with the different thickness of emissive layer.
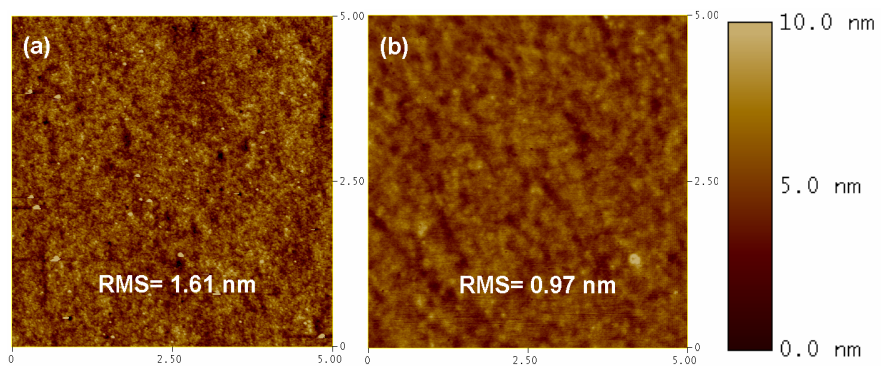
Fig. 1.

PF-FSO10
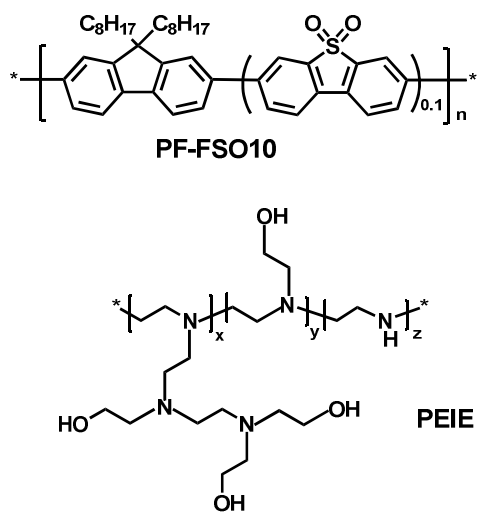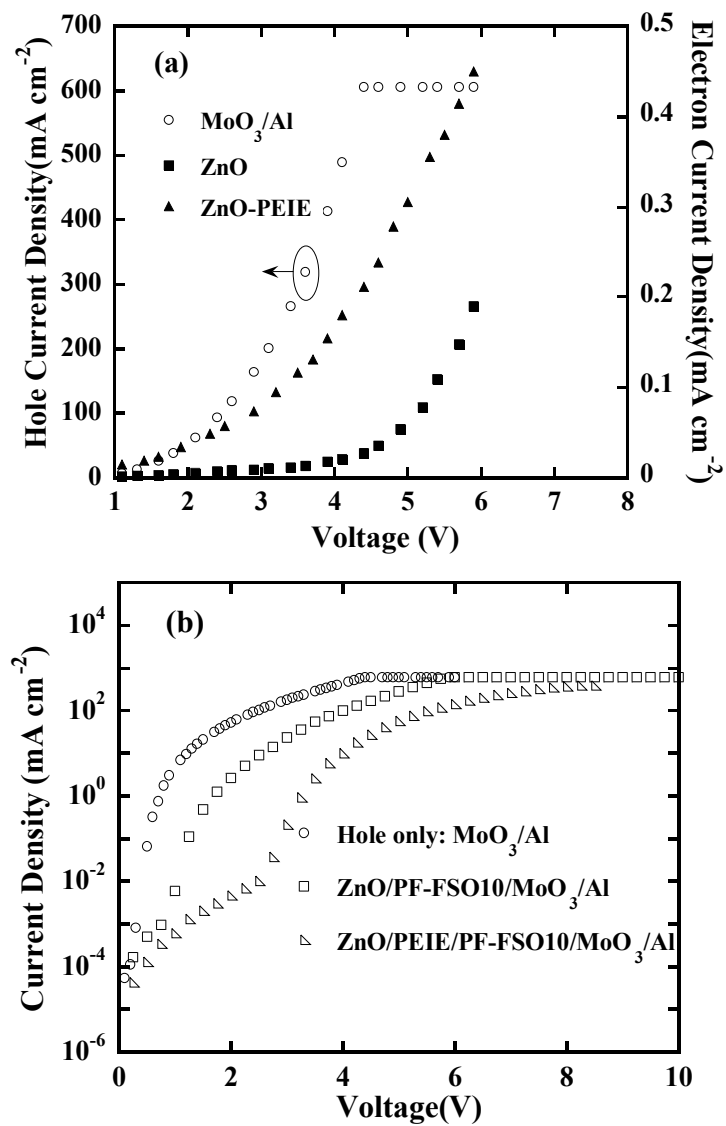
PEIE

Fig. 2.

Fig. 3.
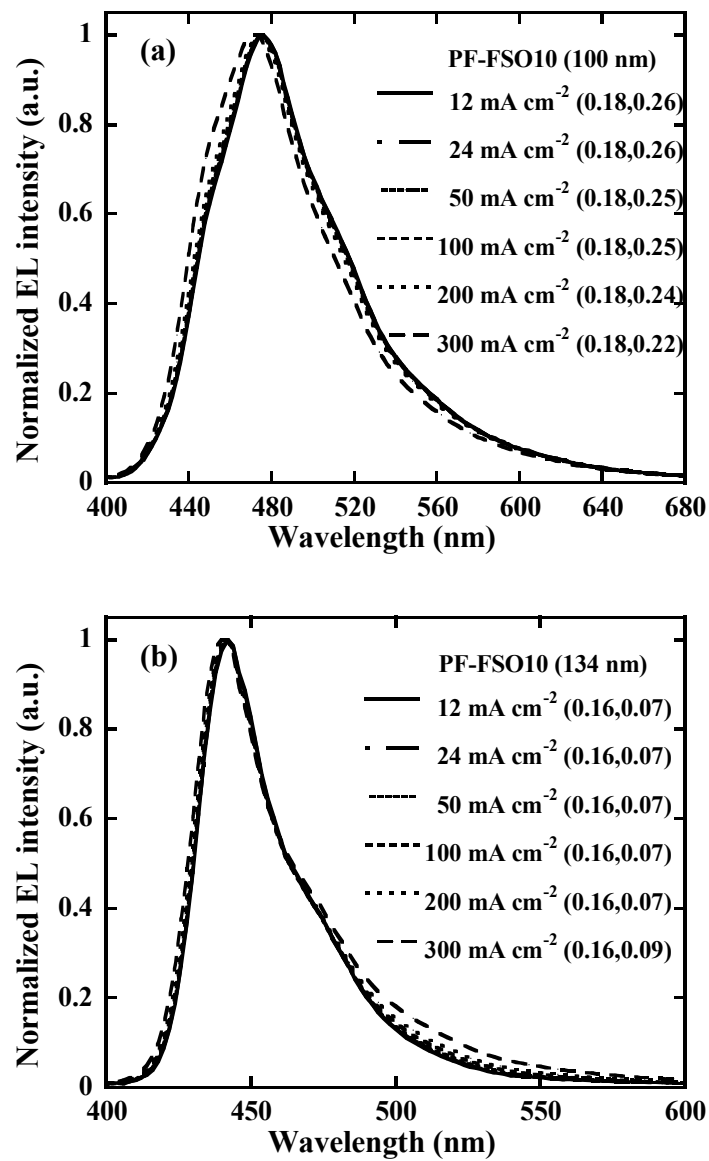
Fig. 4.
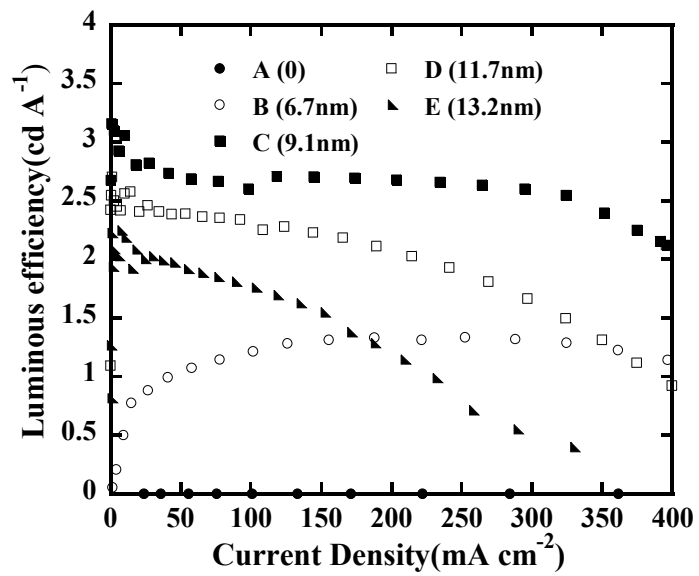
Fig. 5
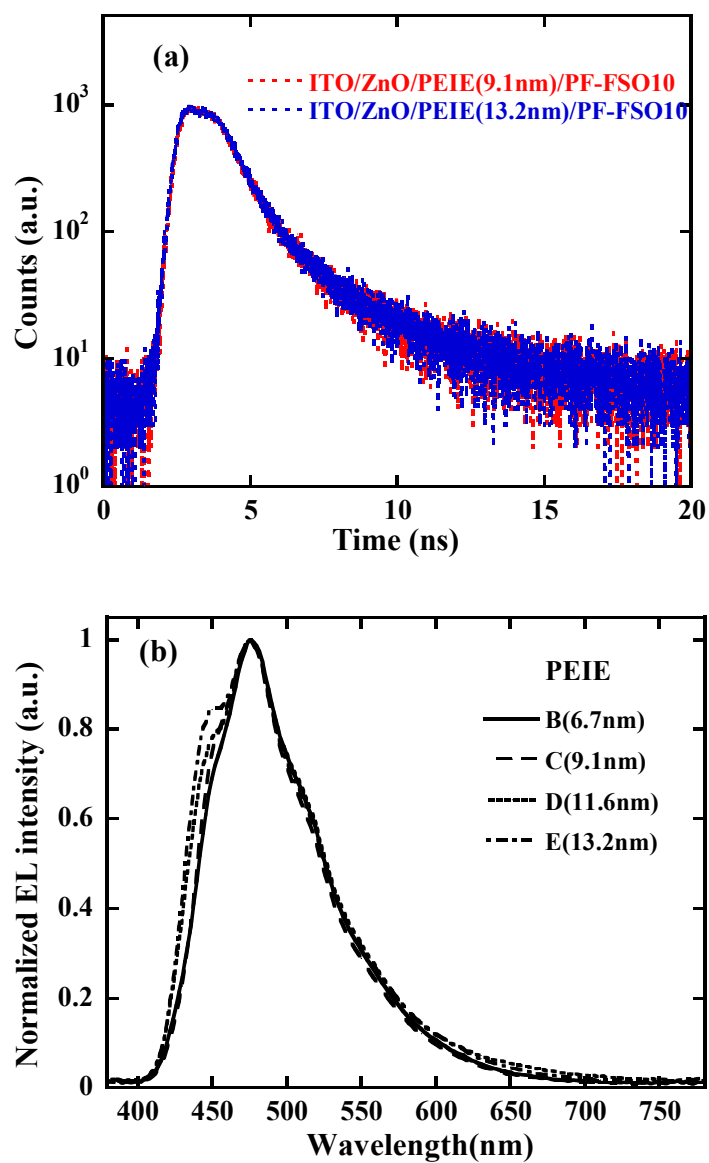
Fig. 6
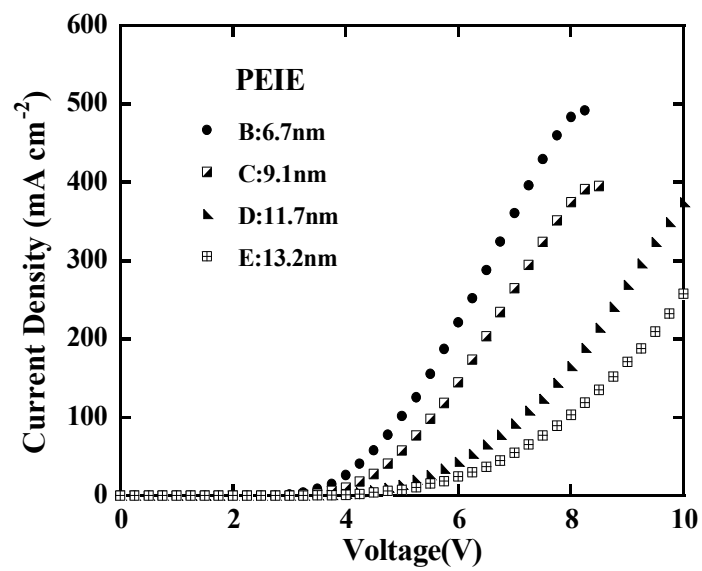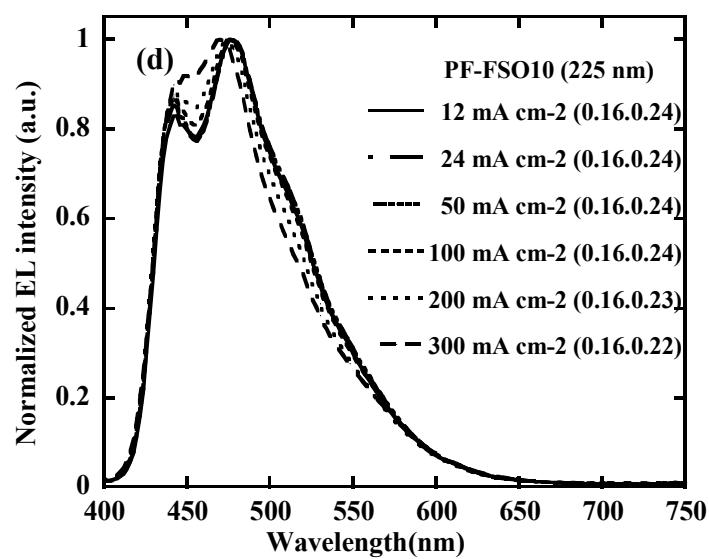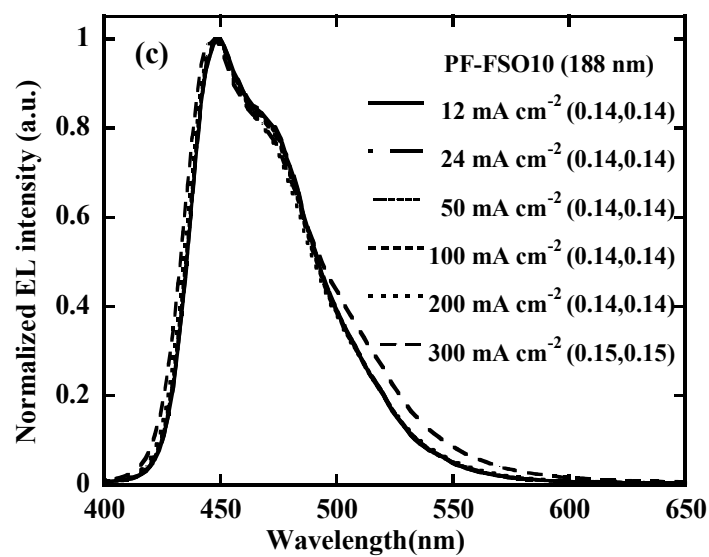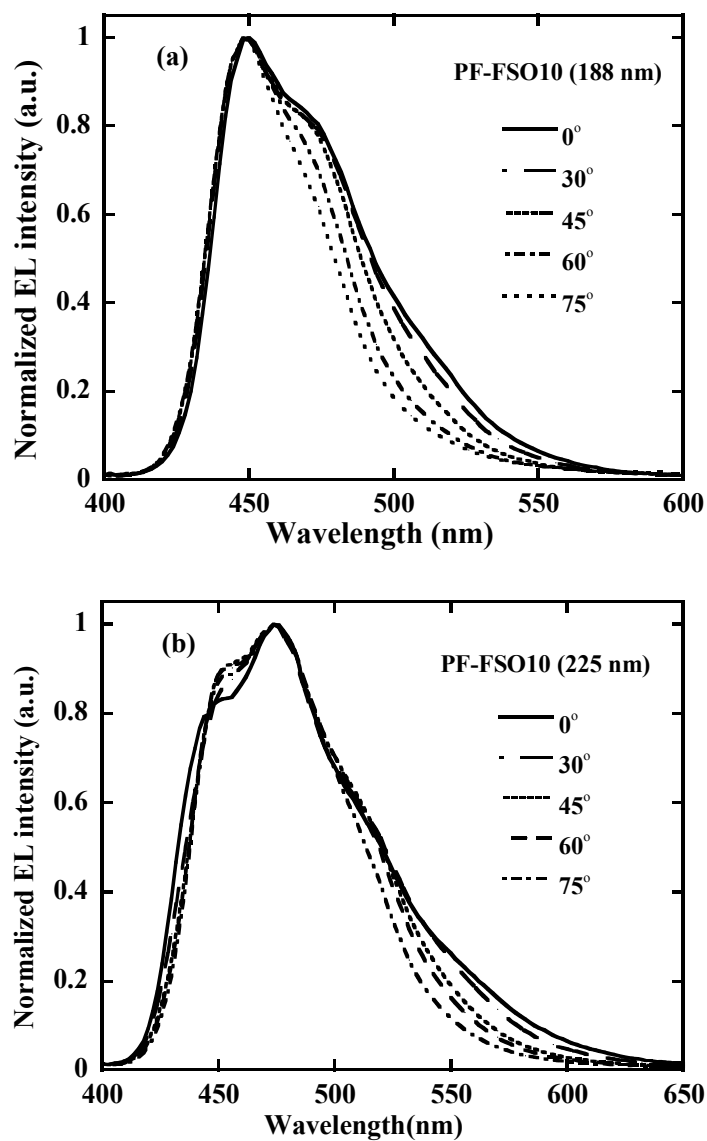
Fig. 7.
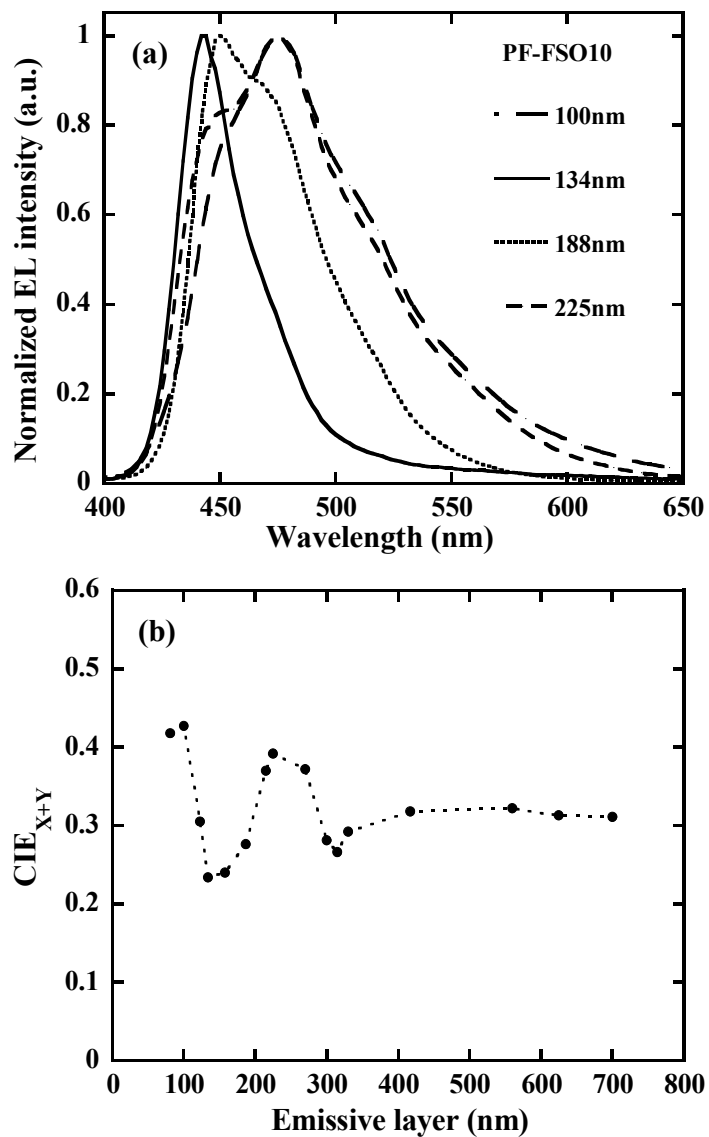
Fig.8

Fig. 9

Table 1 Device parameters with the different PEIE's thickness.

device	PEIE (nm)	V_{on}^a (V)	L_{max}^b (cd m^{-2})	LE_{max}^b (cd A^{-1})	LE^c (cd A^{-1})	CIE^d (x, y)
A	–	6.50	20	3.3×10^{-3}	–	–
B	6.7	3.25	4524	1.33	1.29	(0.19, 0.29)
C	9.1	3.00	8429	3.16	2.60	(0.18, 0.26)
D	11.7	3.25	4935	2.70	1.66	(0.19, 0.26)
E	13.2	3.25	2416	2.23	0.55	(0.19, 0.25)

[a] Defined as the voltage at a luminance of 1 cd m^{-2}; [b] the maxima luminance (cd m^{-2}) and luminous efficiency (cd A^{-1}); [c] luminous efficiency recorded at 300 mA cm^{-2}; [d] color coordinates measured at J = 10 mA cm^{-2}.

Table 2 PL efficiency based on different interfaces

device	Φ_{PL} (%)
Quartz/PF-FSO10(10nm)	47
ITO/ZnO/PF-FSO10(10nm)	24
ITO/ZnO/PEIE(9.1nm)/PF-FSO10(10nm)	34

Table 3 Device performances with the different thickness of emissive layer

thickness	V_{on}[a]	L_{max}[b]	LE_{max}[b]	EQE_{max}[b]	PE_{max}[b]	LE[c]	CIE[d]
(nm)	(V)	(cd m^{-2})	(cd A^{-1})	(%)	(lm W^{-1})	(cd A^{-1})	(x, y)
100	3.0	8429	3.16	2.21	3.05	2.74	(0.18, 0.26)
134	3.4	2262	1.77	3.23	1.24	1.46	(0.16, 0.07)
158	3.8	2934	2.54	3.83	1.50	1.92	(0.15, 0.09)
188	4.0	2932	3.73	4.17	1.89	3.18	(0.14, 0.14)
215	4.0	5162	4.74	4.31	2.60	4.07	(0.15, 0.22)
225	4.0	5403	5.52	4.20	2.97	4.88	(0.16, 0.24)
330	5.4	3201	4.48	4.70	1.56	3.68	(0.14, 0.15)
560	8.4	2372	4.89	4.68	0.92	3.88	(0.16, 0.16)
700	9.2	1112	5.70	5.83	1.21	3.78	(0.16, 0.16)

[a] Defined as the voltage at a luminance of 1 cd m^{-2}; [b] the efficiencies of L, LE, PE and EQE at the maxima for each device; [c] the luminous efficiency (cd A^{-1}) at a luminance of 1000 cd m^{-2}; [d] color coordinates measured at J = 10 mA cm^{-2}.

26

Graphical Abstract

Color Tuning in Inverted Blue Light-Emitting Diodes Based on Polyfluorene Derivative by Adjusting the Thickness of Light-Emitting Layer

Jin Xu, Lei Yu, Liwen Hu, Ruifeng He,* Wei Yang,* Junbiao Peng and Yong Cao

The EL spectra possessed highly adjustability with the variation of thickness of emissive layer in the IPLEDs.